Dynamics and wettability of petroleum fluids in shale oil probed by 2D T1 -T2 and fast field cycling NMR relaxation

Jean-Pierre Korb, B. Nicot, I. Jolivet

Dynamics and wettability of petroleum fluids in shale oil probed by 2D T_1-T_2 and fast field cycling NMR relaxation

J.-P. Korb[a,b,+], B. Nicot[c], I. Jolivet[c]

[a]Physique de la Matière Condensée, Ecole Polytechnique-CNRS, 91128 Palaiseau, France.

[b]Sorbonne Université, UPMC Univ. Paris 06, Laboratoire Physicochimie des Electrolytes, Nanosystèmes Interfaciaux (Phenix), Paris Cedex 5, France.

[c]Total EP, Centre Scientifique et Technique Jean Feger (CSTJF), 64018 Pau, France.

Abstract

We present nuclear magnetic relaxation dispersion of longitudinal relaxation rates $1/T_1$ (NMRD) and 2D spin-correlation T_1-T_2 at different frequencies for oil and brine confined in shale oil rocks. We describe the nuclear spin relaxation models used for obtaining important dynamical and structural parameters from these experiments. These models allow interpreting the very different T_1/T_2 ratio observed for these petroleum fluids on the 2D spin-correlation T_1-T_2 observed at two frequencies. They give also new informations on the dynamics and wettability of the embedded fluids as well as some structural measurement on the kerogen pore size.

Keywords: Shale oil rocks, FFC relaxometry, oil and brine dynamics, wettability

[+] Corresponding author

E-mail address: jean-pierre.korb@polytechnique.fr

Tel: 33 1 69 33 47 39

1. Introduction

It is of primary importance to probe *in situ* and non-invasively the dynamics and wettability of oil, water and gas trapped in the complex microstructure of shale-oil rocks. The main reason is because liquid and gas hydrocarbons can be produced from these organic and mineral sedimentary rocks. However, most of the usual techniques cannot separate these fluids in the complex microstructure of shale rocks. Several attempts of one-dimensional (1D) and two-dimensional (2D) low-field ^{1}H nuclear magnetic resonance (NMR) techniques have proven useful for probing the fluid dynamics in mature organic-shale reservoir rocks [1-3]. 2D spin-correlation NMR technique at low fields (T_1-T_2) has proven useful for separating fluids in confinement [4] and can be made down-hole. Recently, we have used this 2D NMR technique for probing the saturation of oil and brine in shale rocks [5]. However, it is not directly sensitive to the dynamics of the embedded liquids. We have also evidenced by fast-field cycling relaxometry strongly different magnetic-field dependence (NMRD) of the longitudinal nuclear-spin-lattice relaxation rate $1/T_1$ of oil and and brine embedded in shales [5]. As this technique explores a large magnetic field range allowing changing the fluctuations to which the nuclear spin relaxation is sensitive, it has offered multiscale opportunities for characterizing the molecular dynamics and transport properties of fluids embedded in confined environments [6]. But some questions still remain for interpreting the striking differences in the NMRD profiles as well as the far different T_1/T_2 ratio in the (T_1-T_2) data of oil and brine in shales. Here, we come back to the necessary theoretical models in 1D and 2D NMR data used at variable frequencies for obtaining some new dynamical and structural information on the mineral (clay) and organic (kerogen) microstructures.

2. Materials and methods

The rocks samples (oil/water/air and water/air) come from a field producing light oil and are supplied by *Total EP, France*. The sponge-like microstructure of kerogen has been characterized with FIB SEM technique and presents a fractal distribution of pore sizes with a huge surface area [7, 8]. We show in Fig.1 FIB SEM micrograph of the microporosity of a shale oil rock sample evidencing the quasi 1D

connectivity of the kerogen micropores. Electron Spin Resonance (ESR) spectroscopy has determined a density of $\eta_S=4.50\times10^{19}$ paramagnetic species (mainly Mn^{2+} ions) per gram of shale-oil sample in a single environment [5]. The analysis has revealed a density of $\rho_{Shale}\sim2.6\ g/cm^3$. We have deduced a surface density of paramagnetic relaxation sinks $\sigma_s=(\eta_S\rho_{Shale})^{2/3}=2.39\times10^{13}\ Mn^{2+}/cm^2$ assuming a homogeneous repartition in the sample. This gives an average distance between relaxing sinks about $1/\sqrt{\sigma_s}\sim 2\ nm$ on pore surfaces. NMRD data have been performed on oil/water/air shale rocks at room temperature with a fast-field cycling (FFC) spectrometer from *Stelar s.r.l., Mede, Italy* [5]. For separating the NMRD responses of confined oil and water, we have used a standard procedure in the petroleum industry [5]. Last, we used *2D* NMR T_1-T_2 correlation experiments performed at 2.5 MHz and 23 MHz with an *Oxford Instrument* spectrometer on "as received" oil/water/air shale rock which presents two different peaks associated to confined oil and water (brine).

3. Experimental results, data treatment and discussion on NMRD in shales

We used a home-written "Matlab" program [5] following closely the Butler-Reeds-Dawson [9] and Venkataramanan *et al* algorithms [10] for analyzing the longitudinal magnetization decays ending to a bimodal distribution of T_1 for all the Larmor frequencies studied between 10 kHz and 35 MHz. As shown in inset of Fig. 2, the two thin peaks allow building two different T_1-NMRD profiles assigned to oil and water [11]. We have proposed theoretical models for describing the longitudinal and transverse nuclear spin relaxation of a fluid embedded either in 2D [12-14] or 1D [15] pore geometries. Here, we just outline the essential features of these models for water and oil fluids in confinement.

3.1 NMRD profile of water confined in lamellar clay minerals

We assume the general biphasic fast exchange model where the exchange time between the proton-water transiently belonging to the surface and the bulk in pores is shorter than their respective relaxation times. When considering the lamellar clay mineral modeled as a 2D system, the main contribution of the proton relaxation comes from the 2D translational proton-water *(I)* diffusion at proximity of the fixed

paramagnetic relaxing sinks (Mn^{2+}) of spins *S=5/2* that modulates their relative dipole-dipole interaction. The numerous 2D molecular reencounters (^1H-Mn^{2+}) are responsible for the net frequency dependence observed in Fig. 2. In that case, we have previously found that the longitudinal and transverse relaxation times are given by [12-14]:

$$R_{1,water}(\omega_I) = R_{1,bulk} + \left[\pi/\left(30\delta_{water}^3\right)\right]\sigma_S\rho_{water}S_{p,NMR}(\gamma_I\gamma_S\hbar)^2 S(S+1)\tau_m \times\left[3\ln\left(\frac{1+\omega_I^2\tau_m^2}{(\tau_m/\tau_s)^2+\omega_I^2\tau_m^2}\right)+7\ln\left(\frac{1+\omega_S^2\tau_m^2}{(\tau_m/\tau_s)^2+\omega_S^2\tau_m^2}\right)\right]. \quad (1)$$

$$R_{2,water}(\omega_I) = R_{2,bulk} + \left[2\pi/\left(30\delta_{water}^3\right)\right]\sigma_S\rho_{water}S_{p,NMR}(\gamma_I\gamma_S\hbar)^2 S(S+1)\tau_m \times\left[2Ln\left(\frac{\tau_S}{\tau_m}\right)+\frac{3}{4}\ln\left(\frac{1+\omega_I^2\tau_m^2}{(\tau_m/\tau_s)^2+\omega_I^2\tau_m^2}\right)+\frac{13}{4}\ln\left(\frac{1+\omega_S^2\tau_m^2}{(\tau_m/\tau_s)^2+\omega_S^2\tau_m^2}\right)\right] \quad (2)$$

In Eqs. 1 and 2, γ_I and γ_S =658 γ_I are the gyromagnetic ratio of the proton and electron, σ_S is the surface density of paramagnetic sources of relaxation that we can probe by electron spin resonance [5] and ρ_{water} is the water density. Here, we have considered a thin surface layer λ of the order of a molecular size, δ_{water}*~0.3 nm*. This distance corresponds also to the average distance of minimal approach between proton-water and Mn^{2+} ions. The translational correlation time τ_m is associated with individual water molecular jumps at pore surfaces. The surface residence time, τ_s *(*$>>\tau_m$*)*, which is limited by the molecular desorption from the surface layer λ controls how long the proton species *I* and *S* stay correlated at pore surfaces. The ratio τ_s/τ_m thus represents the dynamical surface affinity or NMR wettability [14]. The best fit obtained with Eq. 1 is displayed in Fig. 2 with a NMR specific surface area $S_{p,NMR}$*=47* m^2/g, τ_m*=12.0 ps* and the frequency independent bulk value $R_{1,bulk}^{water} \approx 30 s^{-1}$. For taking into account the rather dispersed data at low frequency, we have varied the activation energy $5 \le E_S \le 7.5$ *kcal/mol* associated to the activated residence times $\tau_S = \tau_{S0}\, exp(E_S/RT)$ at pore surfaces. At high frequency (ω_I*>0.3* MHz) the entire fitting curves merge to a single one characterized by a single time of residence τ_s*=0.6* μ*s (*$\tau_s >> \tau_m$*)* consistent with a water-wet situation (Fig. 2). An estimation of the translational diffusion coefficient of

water at the mineral clay-like surface thus gives $D_{surf}=\delta_{water}^2/(4\tau_m)=1.88\times10^{-5}$ cm^2/s which is slightly lower than what is expected for bulk water at T=25°C.

3.2 NMRD profile of oil confined in the microstructure of kerogen.

Based on our previous proton NMRD data in 1D pores [15], the inverse squared-root behavior with a leveling-off at low frequency shown as a red line in Fig. 2 strongly supports a relaxation process induced by a quasi-1D-translational diffusion of proton-oil species in proximity of paramagnetic Mn^{2+} ions at surface of kerogen micropores with an exponential cut-off after a surface time of residence τ_S. Here again, the dominant feature of this relaxation process is the time dependence of the probability of reencounters between moving protons *I* and fixed paramagnetic spins *S* evolving at long times as $P(\tau)\propto exp(-\tau/\tau_S)/\sqrt{(\tau/\tau_m)}$. This gives the behavior $R_1\propto 1/\sqrt{\omega_I}$ observed in Fig. 2 at high frequency. The measured fractal pore-size distribution gives a number of pores $N(R)\propto(R/R_{max})^{-Df}$ of size *R* in the range $\{R_{min}\sim 2.5$ *nm* - $R_{max}\sim 630$ *nm*$\}$ with the fractal dimension $D_f\sim 2.3$ [7, 8]. Due to the divergence of such a distribution for small nanopores, one finds that the highest number of pores *N(R)* is around *R~2.5-3 nm*. The following relations proposed [15] for the longitudinal and transverse relaxation rates induced by a translational diffusion of a liquid confined in 1D cylindrical nanopores allows reproducing almost all the features shown in Fig. (2):

$$R_{1,oil}(\omega_I)=R_{1,bulk}^{oil}+\sqrt{2}/\left(15\pi R\delta_{1D,oil}^2\right)\sigma_s\rho_{oil}S_{p,NMR}\left(\gamma_I\gamma_S\hbar\right)^2S(S+1)\sqrt{\tau_m\tau_s}\times\left[\frac{3\sqrt{1+\sqrt{1+\omega_I^2\tau_s^2}}}{\sqrt{1+\omega_I^2\tau_s^2}}+\frac{7\sqrt{1+\sqrt{1+\omega_S^2\tau_s^2}}}{\sqrt{1+\omega_S^2\tau_s^2}}\right] \quad . \qquad (3)$$

$$R_{2,oil}(\omega_I)=R_{2,bulk}^{oil}+2\sqrt{2}/\left(15\sqrt{2}\pi R\delta_{1D,oil}^2\right)\sigma_s\rho_{oil}S_{p,NMR}\left(\gamma_I\gamma_S\hbar\right)^2S(S+1)\sqrt{\tau_m\tau_s}\times\left[1+\frac{\sqrt{1+\sqrt{1+\omega_I^2\tau_s^2}}}{\sqrt{1+\omega_I^2\tau_s^2}}+\frac{13\sqrt{2}}{8}\frac{\sqrt{1+\sqrt{1+\omega_S^2\tau_s^2}}}{\sqrt{1+\omega_S^2\tau_s^2}}\right]. \qquad (4)$$

In Eqs. 3 and 4, the oil density is $\rho_{oil} = 0.85\ g/cm^3$ and $R \sim 3.0\ nm$ is the pore radius of the largest population of pores following the fractal distribution described above. $\delta_{1D,oil} \sim \delta_{oil}/2$ is the distance of minimal approach between *I* and *S* spins where δ_{oil} is the average size of hydrocarbon (octane). This distance is taken at half of the molecular size because the saturated oil has no ligand field to the paramagnetic source of relaxation. The continuous curves of Fig. 2 have been fitted with Eqs. 3 and 4, with $S_{p,NMR} = 30\ m^2/g$ and $\tau_m = 4.1\ ns$ for different values of the activation energy $6.6 \leq E_S \leq 7.4\ kcal/mol$ associated to the activated time of residence $\tau_S = \tau_{S0}\ exp(E_S/RT)$ for considering the rather dispersed data at low frequency. We see that such a distribution of E_S only affects the NMRD profile $1/T_1(\omega_I)$ below 0.3 MHz. In the high frequency range where all the fits merge to a single theoretical profile $1/T_1(\omega_I) \propto 1/\sqrt{\omega_I}$, we find a single surface residence time $\tau_s \sim 0.78\ \mu s$. An estimation of the translational diffusion coefficient of oil at the surface of kerogen pores thus gives $D_{surf} = \delta_{oil}^2/(4\tau_m) = 2.58 \times 10^{-7} cm^2/s$. We have introduced previously a dynamical surface affinity index $A = \tau_s/\tau_m$ that qualifies an average number of molecular steps on the pore surface giving a kind of local NMR wettability [14]. Here, we find $A \sim 195$ which is typical of an oil-wet situation in kerogen pores. The very small value of D_{surf} compared to the bulk octane is due to the oil-wet condition favouring the dynamical surface affinity of the highly confined oil in kerogen nanopores.

4. Experimental results, data treatment and discussion on 2D NMR T_1-T_2 and T_1/T_2 in shales

The confined oil population has elongated peaks in Fig. 3a, b which exhibits a surprisingly high T_1/T_2 ratio around 10 at 2.5 MHz and around 40-50 at 23 MHz. On the contrary, the water peak stays fixed around $T_1/T_2 \sim 1.4$. The high T_1/T_2 ratio could reveal viscous bitumen [1]. This hypothesis should be discarded due to the high ratio around 4-5 in presence of light oil [11]. Moreover, we did not observe by ESR the typical paramagnetic impurities of bitumen. In Figs. 3, we do not observe any cross peaks, thus proving the absence of proton exchange between oil and water populations on the time scale of 2D NMR

experiment. One obtains from Eqs. (1-4) the following ratio of $T_{1,water}^{2D}/T_{2,water}^{2D}$ and $T_{1,oil}^{1D}/T_{2,oil}^{1D}$ for 2D and 1D pore-geometries, respectively:

$$\frac{T_{1,water}^{2D}}{T_{2,water}^{2D}} \approx 2\frac{\left[2Ln\left(\frac{\tau_S}{\tau_m}\right)+\frac{3}{4}\ln\left(\frac{1+\omega_I^2\tau_m^2}{(\tau_m/\tau_s)^2+\omega_I^2\tau_m^2}\right)+\frac{13}{4}\ln\left(\frac{1+\omega_S^2\tau_m^2}{(\tau_m/\tau_s)^2+\omega_S^2\tau_m^2}\right)\right]}{\left[3\ln\left(\frac{1+\omega_I^2\tau_m^2}{(\tau_m/\tau_s)^2+\omega_I^2\tau_m^2}\right)+7\ln\left(\frac{1+\omega_S^2\tau_m^2}{(\tau_m/\tau_s)^2+\omega_S^2\tau_m^2}\right)\right]}, \quad (5)$$

$$\frac{T_{1,oil}^{1D}}{T_{2,oil}^{1D}} \approx 2\sqrt{2}\frac{1+\left(3\sqrt{2}/8\right)\sqrt{1+\sqrt{1+\omega_I^2\tau_s^2}}/\sqrt{1+\omega_I^2\tau_s^2}+\left(13\sqrt{2}/8\right)\sqrt{1+\sqrt{1+\omega_S^2\tau_s^2}}/\sqrt{1+\omega_S^2\tau_s^2}}{3\sqrt{1+\sqrt{1+\omega_I^2\tau_s^2}}/\sqrt{1+\omega_I^2\tau_s^2}+7\sqrt{1+\sqrt{1+\omega_S^2\tau_s^2}}/\sqrt{1+\omega_S^2\tau_s^2}}. \quad (6)$$

We remind that the 1D diffusion relaxation model presented in Section 3.2 for oil supposes a very long surface residence time τ_s *(>> τ_m)* [5]. For the observed oil data, it appears from Eqs. 3 and 4 that $T_{1,oil}^{1D} \propto \sqrt{\omega_I/\tau_m}$ independently of τ_S when *1* $\leq \tau_s \leq$ *10* μs, while T_2 behaves as $T_{2,oil}^{1D} \propto 1/\sqrt{\tau_m \tau_S}$ for all τ_s. This gives a ratio that behaves as $T_{1,oil}^{1D}/T_{2,oil}^{1D} \to 1$ when $\omega_I \to 0$ and $T_{1,oil}^{1D}/T_{2,oil}^{1D} \propto \sqrt{\omega_I \tau_S}$ at high frequency while $T_{2,water}^{2D}/T_{2,water}^{2D} \approx 1.4$ for water. We have displayed in Fig. 4a the frequency dependencies of T_1/T_2 for water (Eq. 5) and oil (Eq. 6) when varying τ_s in the range between *1* μs and *10* μs considering the large variety of oil surface dynamics in the kerogen pores. One notes that this ratio for oil could reach the values around *4-10* at *2.5 MHz* and *40-50* at *23 MHz*. For water, the ratio $T_{2,water}^{2D}/T_{2,water}^{2D} \approx 1.4$ does not vary much in frequency (or in τ_s) due to the 2D diffusive dimension and the small range of pore sizes.

Last, we have also displayed in Fig. 4b the 2D spin-correlation map T_1-T_2 calculated at *2.5* and *23 MHz* with Eqs. 1-4 by varying τ_m within *{0.1-10 ns}* and {*10-100 ps}* for oil and water, respectively. We note that Fig. 4b reproduces the two following relaxation features. (i) The oil peak shifts as $T_{1,oil}^{1D} \propto \sqrt{\omega_I \tau_S} T_{2,oil}^{1D}$ in the range of large T_1 and T_2 values when increasing the frequency in excellent agreement with the proposed 1D relaxation theory. We have represented schematically in Fig. 4b the leveling off $T_{1,oil}^{1D} \propto \sqrt{\omega_I/\tau_m}$ where T_1 appears to be independent of T_2 within the short T_1 and T_2 values.

This leveling off is consistent with the general observation in shale oil rocks [11]. (ii) The evolution of the central peak of the T_1-T_2 correlation map as well as the large value observed for T_1/T_2 (Fig. 4a) can thus be explained by the low dimensionality of the oil diffusion at the huge kerogen pore surface. This result is of particular importance because it shows that measuring T_1-T_2 at different frequencies can inform on the fluid typing in confinement.

We discuss finally how to generalize our observed NMRD profiles to other shale samples. The kerogen maturity can have a direct effect on the specific surface area $S_{p,NMR}$ of the kerogen because it will develop more and more sponge-like porosity. As $R_{1,oil} \propto S_{p,NMR}$, the NMRD profile will thus be linearly dependent on the kerogen maturity. The value $S_{p,NMR} = 30\ m^2/g$ used in our study is typical of a mature sample compared to a much lower value found for a weak kerogen maturity. Varying the nature (spin value S) and quantity (surface density σ_S) of paramagnetic sources of relaxation will only affect the absolute value of $R_{1,oil}$ but not its frequency dependence. The distribution of times of residence τ_S for oil at pore surfaces (Fig. 2) at low frequency can be universally encountered in other shale samples. Even, if the NMRD data are spatially limited to a few nanopores, the evidence of such a distribution at long times is consistent with the recent simulations and theoretical calculations proposed by several authors for interpreting the difficulty of expelling the petroleum fluids from the kerogen microstructure [16].

5. Conclusion

We have shown that fast-field-cycling NMR relaxometry allows probing non-invasively surface diffusion coefficients, residence times and local wettability of oil and water (brine) embedded in shale rocks. The high T_1/T_2 values found for oil are shown to be due to a lower diffusion dimensionality (~1D) than for water (2D) and no bitumen presence has been required. Last, we have shown that measuring the 2D spin-correlation spectra T_1-T_2 at two frequencies gives confidence on fluid typing in the high confinement of shales. We believe that the frequency dependencies of the NMRD profiles which depend drastically on the pore geometry and local dimensionality give unambiguous information on the local dynamics of the embedded petroleum fluids.

REFERENCES

[1] P.M. Singer, E. Rylander, T. Jiang, R. McLin, R.E. Lewis, S.M. Sinclair, Society of Core Analysts, SCA2013-018.

[2] A.E. Ozen, R.F. Sigal, Petrophysics, 54 (2013) 11-19.

[3] E. Odusina, C. Sondergeld, C. Rai, Society of Petroleum Engineers, (2011) paper SPE147371.

[4] M. D. Hürlimann, L. Venkataramanan, J. Magn. Reson., 157 (2002) 31-42.

[5] J.-P. Korb, B. Nicot, A. Louis-Joseph, S. Bubicci, G. Ferrante, J. Phys. Chem. C., 118 (2014), 23212-23218.

[6] R. Kimmich, E. Anoardo, Prog. Nucl. Magn. Reson. Spectrosc, 44 (2004) 257−320.

[7] M.E. Curtiss, R.J Ambrose, C.H. Sondergeld, Ch. Rai, http://www.ogs.ou.edu/MEETINGS/Presentations/ShalesMoving2011/CurtisMicro.pdf (2011).

[8] M.E. Curtiss, R.J. Ambrose, Ch. Rai, CUSG/SPE (2010), 137693.

[9] J.-P. Butler, J.A., Reeds, , S.V. Dawson, SIAM J. Numer. Anal**.,** 18 (1981) 381-397.

[10] L. Venkataramanan, Y.Q. Song, M.D. Hürlimann, IEEE Trans. Signal Proc., 50 (2002) 1017-1026.

[11] B. Nicot, N. Vorapalawut, B. Rousseau; L.F. Madariaga, G. Hamon, J.-P. Korb, Petrophysics, 15 (2015) 19-29.

[12] F. Barberon, J.-P. Korb, D. Petit, V. Morin, E. Bermejo, Phys. Rev. Lett., *90*, (2003) 1-4.

[13] J.-P. Korb, M. Whaley-Hodges, R.G. Bryant, Phys. Rev. E, *56*, (1997) 1934-1944.

[14] J.-P. Korb, G. Freiman, B. Nicot, P. Ligneul, Phys. Rev. E, 80 (2009) 061601-061612.

[15] F. Dalas, J.-P. Korb, S. Pourchet, A. Nonat, D. Rinaldi, J. Phys. Chem. C, 118 (2014) 8387-8396.

[16] Th. Lee, L. Bocquet, B. Coasne, Nature comm., DOI; 10.1038/ncomms (2016) 11890.

Figure captions

Fig. 1 (a) FIB SEM micrographs of the microporosity of a shale oil rock sample.

Fig. 2 Logarithmic plot of the measured proton spin−lattice relaxation rate constants R_1 as a function of the proton Larmor frequency for oil/water/air shale. The continuous blue (water) and red (oil) lines are the best fits obtained with Eqs. 1 and 3, with the values obtained for τ_m and τ_S. We have varied the activation energy E_s at low frequency. We show in inset some examples of the bimodal T_1-distributions obtained at different frequencies.

Fig. 3 (a) Two-dimensional T_1-T_2 spin-correlation maps observed for water and oil on "as received" shale-oil rock measured at 2.5 MHz. **(b)** *ibid* T_1-T_2 data measured at 23 MHz. The dashed lines indicate the values of T_1/T_2 ratio.

Fig. 4 (a) Theoretical dependencies of the ratio T_1/T_2 with Larmor frequency for a 2D diffusion of water in lamellar clay mineral (Eq. 5) and a 1D diffusion of oil in kerogen pores (Eq. 6). The circular points are the experimental values observed at 2.5 and 23 MHz for oil in kerogen. The different continuous lines correspond to different values of $0.1 \leq \tau_S \leq 1\ \mu s$. **(b)** Theoretical *2D* T_1-T_2 spin-correlation maps calculated from Eqs. 1-4 at 2.5 and 23 MHz by varying τ_m within *{0.1-10 ns}* and {*10-100 ps}* for oil and water, respectively. We have represented schematically in dotted lines the leveling off $T_{1,oil}^{1D} \propto \sqrt{\omega_I / \tau_m}$ where T_1 appears to be independent of T_2 for short T_1 and T_2 values.

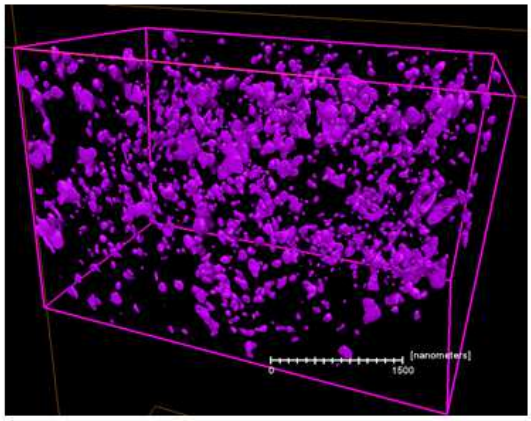

Fig. 1

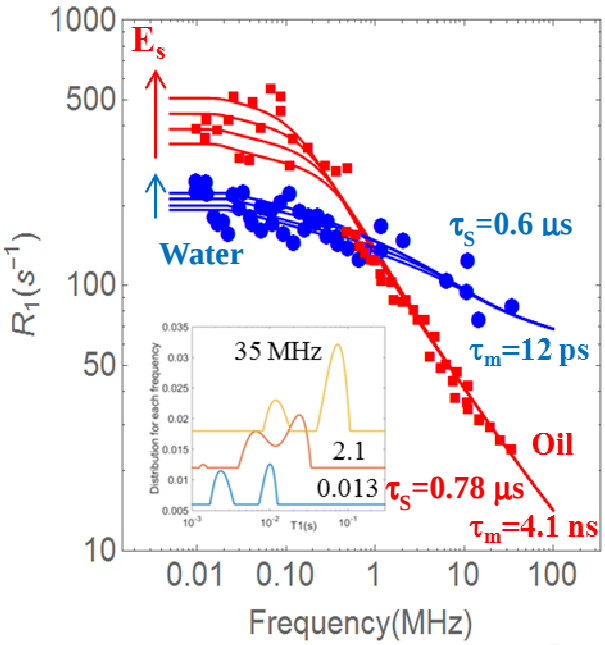

Fig. 2

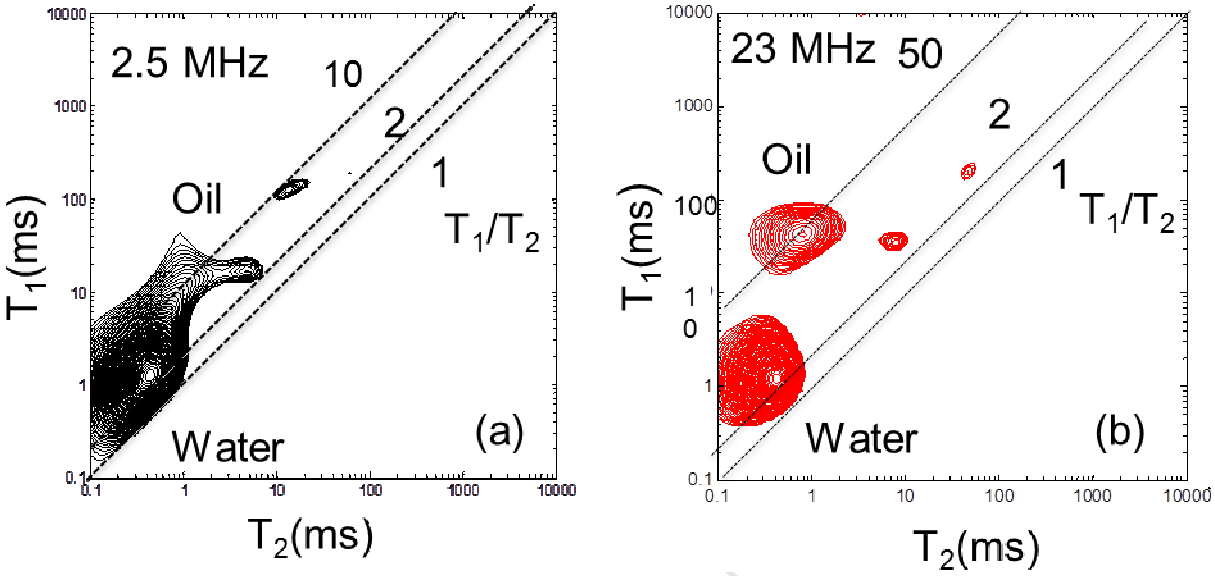

Fig. 3

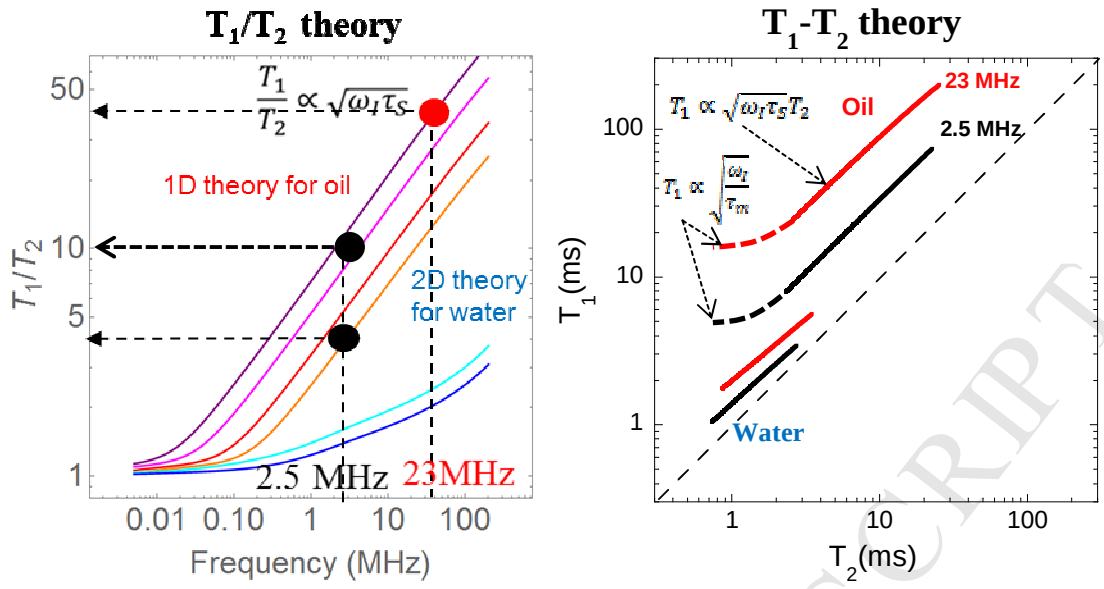

Fig. 4

Graphical abstract

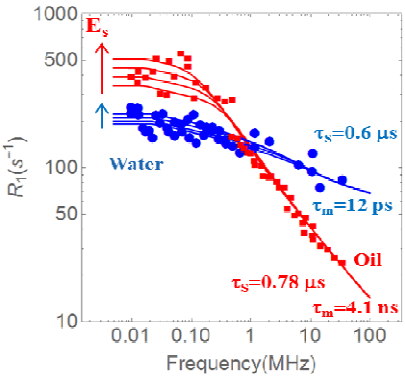

Highligths

- Nuclear magnetic relaxation dispersion profiles of longitudinal relaxation rates $1/T_1$ (NMRD) of oil and brine confined in shale oil rocks.
- Description of the nuclear relaxation models used for obtaining important dynamical and structural parameters from these experiments.
- New interpretation of the very different T_1/T_2 ratio observed for these petroleum fluids on the 2D spin-correlation maps T_1-T_2 observed at two frequencies.
- New information on the dynamics and wettability of the embedded fluids as well as some structural measurement on the kerogen pore size